International Core Journal of Engineering Volume 12 Issue 5, 2026
ISSN: 2414-1895 DOI: 10.6919/ICJE.202605_12(5).0025

Mechanism Design and Simulation Analysis of an Underactuated Hexapod Robot

Shuowen Gu[1], Xiumin Shi[1,2,3,*], Yuming Qi[1,2,3,*], Zhiguo Yang[1], and Minjun Xu[1]

[1] Tianjin University of Technology and Education, Tianjin 300222, China

[2] Tianjin Key Laboratory of Intelligent Robot Technology and Application, Tianjin 300350, China

[3] Tianjin Bonus Robotics Technology Co..td, Tianjin 300350, China

[*]Corresponding Author: Yuming Qi, Xiumin Shi

Abstract

To reduce the control complexity and algorithm development difficulty of conventional hexapod robots (which require 18 servo motors), a leg mechanism for a hexapod robot based on the underactuated principle was designed using SolidWorks. This design omits the ankle joint servo, instead using a single servo combined with a tendon-driven transmission system to actuate both the knee joint and ankle joint in a coupled manner, while a torsion spring provides the restoring torque required for leg lifting. A kinematic model of the leg was established based on the D-H parameter method, and both forward and inverse kinematic analyses of the foot-end effector were performed. The desired foot-end trajectory was obtained through MATLAB simulation. Dynamic simulation analysis of the mechanical leg mechanism was carried out using ADAMS, which verified the correctness and feasibility of the above underactuated structural design and theoretical model, providing a theoretical basis for the development of a physical prototype of the underactuated hexapod robot.

Keywords

Underactuated; Hexapod Robot; Kinematic Model; ADAMS Analysis.

1. Introduction

With the continuous expansion and deepening of special operation scenarios-such as disaster rescue, planetary exploration, and mountainous material transport in complex unstructured environments-there is a growing demand for mobile robots with higher motion stability, terrain adaptability, and intelligent environmental interaction. In these scenarios, traditional wheeled [1] and tracked [2] robots often struggle to achieve stable and efficient autonomous motion due to their reliance on continuous contact and coupling with ground morphology. Against this backdrop, legged robots, by virtue of their discrete footholds and multi-degree-of-freedom coordinated motion, exhibit significant terrain adaptability. In particular, hexapod robots [3], benefiting from their static stability, excel in crossing ditches, climbing steps, and resisting sudden impacts, and have thus become an important research direction in the field of mobile robotics. In recent years, research institutions worldwide have carried out extensive studies on the mechanism design, gait planning, environmental perception, and control strategies of hexapod robots, continuously pushing them toward lighter weight, higher energy efficiency, stronger adaptability, and intelligent coordination to meet the increasingly demanding requirements of special operations [4-6].

ISSN: 2414-1895 DOI: 10.6919/ICJE.202605_12(5).0025

Researchers in Japan have combined a hexapod bio-inspired robot with two advanced detection technologies to build a hexapod mobile robot platform for nuclear facility decommissioning or radiation monitoring [7]. In 2018, the National Technical University of Athens introduced an electro-hydraulically actuated hexapod robot for underwater and seabed operations [8]. The ANYmal robot developed by ETH Zurich features highly elastic joint structures, enabling excellent adaptability and motion efficiency in complex and varied terrains [9]. Inspired by beetles, Zhang Yuhang et al. [10] carried out bionic structural design and improved the robot's maneuverability in unstructured environments through gait simulation. Chongqing University proposed an innovative leg configuration, the LCS-Leg [11], which combines elastic linkages with a tendon-driven mechanism, reducing leg inertia, accelerating response speed, absorbing ground impact via elastic elements, while simultaneously achieving compact structure and high dynamic performance.

Conventional hexapod robots mostly adopt fully actuated designs (three joints per leg), resulting in a large number of joints (18 in total), complex control, heavy body weight, and low energy efficiency. To address these issues, this paper proposes an underactuated leg structure with cable-spring coupling, using only a single servo to drive both the knee and ankle joints in a coupled manner. This design reduces the number of actuators by 33%, lowering weight, cost, and control complexity. Through joint coupling and the passive compliance of the torsion spring, it achieves ground-contact buffering and energy recovery, thereby enhancing adaptability. A corresponding kinematic model is established, followed by mechanical analysis and prototype fabrication. Experiments demonstrate that this solution can stably realize a tripod gait, providing a new approach for developing lightweight, low-cost, and highly adaptable hexapod robots.

2. Leg Mechanism Design

2.1 Design Principles and Overall StructureSection Headings

The robot adopts a bilaterally symmetric hexapod configuration. Each leg mechanism consists of three rotational joints, in which the knee and ankle joints are underactuated and coupled via a cable transmission system. The hip joint axis and knee joint axis are perpendicular to each other, while the knee joint axis and ankle joint axis are parallel to each other. This structure is inspired by underactuated dexterous hands. Compared with conventional hexapod robots that mimic insect structures, the number of servos is reduced by 33%, significantly lowering the control dimensionality and hardware cost(as shown in Fig. 1).

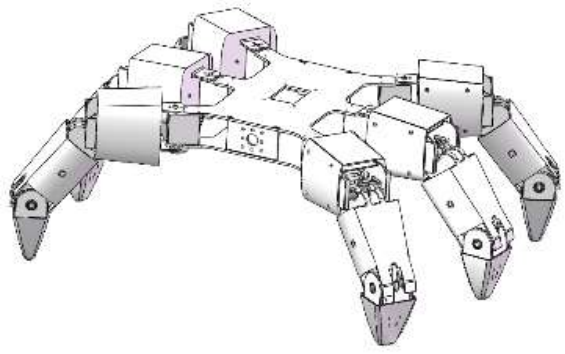

Fig. 1 3D model of the hexapod robot

2.2 Page Numbers

In the underactuated hexapod robot leg, the hip joint motion is directly driven by a high-precision digital servo A, controlling the lateral swing of the leg in the horizontal plane. The knee and ankle joints are coupled via an underactuated cable transmission mechanism. A high-precision digital servo B, located inside the thigh structure, drives a transmission cable through its output pulley. The cable follows a specific topological path: it sequentially passes around the knee joint movable pulley (P_1),

ISSN: 2414-1895 DOI: 10.6919/ICJE.202605_12(5).0025

the guiding fixed pulley (P_3), and the ankle joint fixed pulley (P_2), and is finally anchored to the foot structure. This cable routing ensures that when the knee joint flexes, the cable is effectively tensioned, synchronously driving the ankle joint into dorsiflexion. This "knee-flexion / ankle-dorsiflexion" coupling mechanism forms the core "stance-swing coupling", significantly improving gait efficiency and foot-end trajectory adaptability. The underactuated system incorporates an ankle joint rotation limit mechanism, which restricts the ankle dorsiflexion angle during the initial tensioning phase to prevent undesired upward lifting of the foot end. Meanwhile, high-stiffness torsion springs are integrated onto both the knee and ankle joint shafts, forming an elastic energy storage and passive buffering mechanism (as shown in Fig. 2).

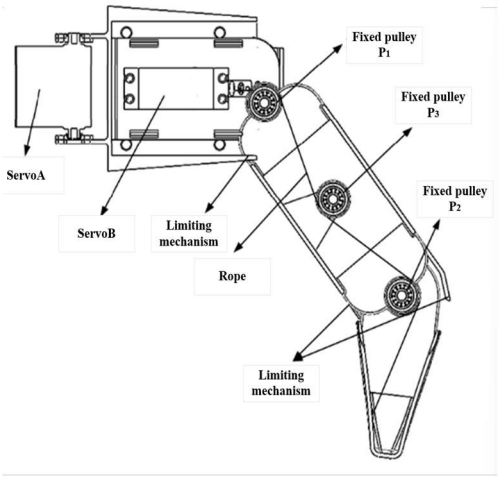

Fig. 2 Schematic diagram of the robot mechanism design

2.3 Structural Parameters of the Hexapod Robot

To clarify the key geometric dimensions and physical characteristics of the designed underactuated hexapod robot, and to facilitate subsequent kinematic modeling, dynamic simulation, and prototype manufacturing, the main structural parameters of this design are shown in Table 1.

Table 1. Main structural parameters of the underactuated hexapod robot

Name	Parameter	Unit
Body length	480	mm
Body width	620	mm
Body height	250	mm
Thigh length	100	mm
Calf length	120	mm
Foot end length	80	mm
Hip joint rotation range	-20-20	°
Knee joint rotation range	20–60	°
Ankle joint rotation range	20–45	°
Servo rated torque	3.5	N·m
Knee joint torsion spring stiffness	0.878	Nm/rad
Ankle joint torsion spring stiffness	0.474	Nm/rad
Total mass	5.2	Kg

ISSN: 2414-1895 DOI: 10.6919/ICJE.202605_12(5).0025

3. Establishment and Analysis of the Kinematic Model of the Underactuated Leg Mechanism

Based on the design, a D-H coordinate system for the underactuated hexapod robot is established, and forward and inverse kinematic solutions are derived [12]. Let the hip joint angle be θ_1, and let the cable extension/retraction length that drives the knee-ankle coupling be s. Let the rotation angle of servo B be φ. Then the system input is (θ_1,φ). The knee joint angle θ_2 and the ankle joint angle θ_3 are not independent variables; they must satisfy the cable length conservation constraint:

$$s = \varphi r_1 = r_2\theta_2 + r_3\theta_3 \tag{1}$$

Let the effective radius of the steering wheel connected to servo B be r_1, the effective radius of the knee joint pulley be r_2, and the effective radius of the ankle joint pulley be r_3.

When the servo pulls the cable to drive the two joints, the ankle joint is first lifted by the cable. When the ankle joint reaches its limit position due to the limit mechanism, the knee joint then begins to rotate. When θ_3 is exactly at its limit position and the knee joint is about to lift, let the cable length at this moment be Δs_1, such that $\Delta s_1 = r_3 \times (\pi/4)$. Therefore, when the cable is retracted by a length Δs, two cases need to be considered:

When $0 \le \Delta s \le \Delta s_1$, the ankle joint has not yet reached its limit position.

$$\begin{cases} \theta_2 = \dfrac{\pi}{9} \\ \theta_3 = \dfrac{\pi}{9} + \dfrac{\Delta s}{r_3} \end{cases} \tag{2}$$

When $\Delta s \ge \Delta s_1$, the ankle joint reaches its limit position.

$$\begin{cases} \theta_2 = \dfrac{\pi}{9} + \dfrac{\Delta s - \Delta s_1}{r_2} \\ \theta_3 = \dfrac{\pi}{4} \end{cases} \tag{3}$$

3.1 Establishment of the Coordinate System for the Front Leg Mechanism

Taking a single leg of the underactuated hexapod robot as an example, D-H modeling is performed for the leg joint links. The D-H coordinate system of a single leg is shown in Fig. 3. Let i represent the i-th joint of the hexapod robot. The D-H parameters are listed in Table 2.

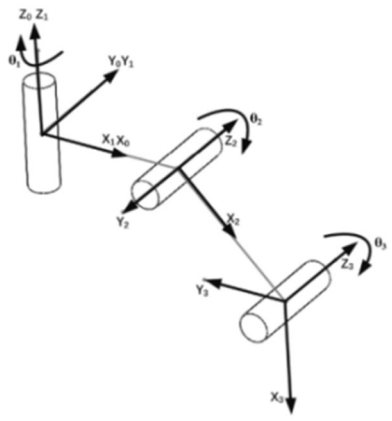

Fig. 3 D-H coordinate system of a single robot leg

ISSN: 2414-1895 DOI: 10.6919/ICJE.202605_12(5).0025

Table 2. Standard D-H coordinate system

Link i	Twist angle αi	Link length αi	Offset di	Joint angle θi
1	-90°	L1	0	θ1
2	0°	L2	0	θ2
3	0°	L3	0	θ3

3.2 Forward Kinematics Analysis of a Single Robot Leg

$$
\begin{aligned}
&{}^{i-1}T_i \\
&= Rot(Z,\ \theta_i)\,Trans(0,0,d_i)\,Trans(a_i,0,0)\,Rot(x,\alpha_i) \\
&= \begin{bmatrix} \cos\theta & -\sin\theta & 0 & 0 \\ \sin\theta & \cos\theta & 0 & 0 \\ 0 & 0 & 1 & 0 \\ 0 & 0 & 0 & 1 \end{bmatrix} \begin{bmatrix} 1 & 0 & 0 & 0 \\ 0 & 1 & 0 & 0 \\ 0 & 0 & 1 & d_i \\ 0 & 0 & 0 & 1 \end{bmatrix} \begin{bmatrix} 1 & 0 & 0 & a_i \\ 0 & 1 & 0 & 0 \\ 0 & 0 & 1 & 0 \\ 0 & 0 & 0 & 1 \end{bmatrix} \begin{bmatrix} 1 & 0 & 0 & 0 \\ 0 & \cos\alpha_i & -\sin\alpha_i & 0 \\ 0 & \sin\alpha_i & \cos\alpha_i & 0 \\ 0 & 0 & 0 & 1 \end{bmatrix} \\
&= \begin{bmatrix} \cos\theta_i & -\sin\theta_i\cos\alpha_i & \sin\theta_i\sin\alpha_i & a_i\cos\theta_i \\ \sin\theta_i & \cos\theta_i\cos\alpha_i & -\cos\theta_i\sin\alpha_i & a_i\sin\theta_i \\ 0 & \sin\alpha_i & \cos\alpha_i & d_i \\ 0 & 0 & 0 & 1 \end{bmatrix}
\end{aligned}
\tag{4}
$$

Substituting the parameters from Table 1 into Equation (4) yields three transformation matrices. The pose of the foot end relative to the base coordinate system is obtained by the chain multiplication of homogeneous transformation matrices:

$$
{}^{0}T_3 = T_1T_2T_3 = \begin{bmatrix} c\theta_1 c(\theta_2+\theta_3) & -c\theta_1 c(\theta_2+\theta_3) & -s\theta_1 & c\theta_1\left[L_1+L_2\,c\theta_2+L_3c(\theta_2+\theta_3)\right] \\ s\theta_1 c(\theta_2+\theta_3) & -s\theta_1 c(\theta_2-\theta_3) & c\theta_1 & s\theta_1\left[L_1+L_2\,c\theta_2+L_3c(\theta_2+\theta_3)\right] \\ -s(\theta_2+\theta_3) & -c(\theta_2-\theta_3) & 0 & -L_3s(\theta_2+\theta_3)-l_2s\theta_2 \\ 0 & 0 & 0 & 1 \end{bmatrix}
\tag{5}
$$

where $c\theta - \cos\theta$; $s\theta - \sin\theta$;

Substituting Equation (4) into Equation (5) yields the forward kinematic model formulas (6) and (7) considering the underactuated coupling:

When $0 \le \Delta s \le \Delta s_1$:

$$
\begin{bmatrix} x \\ y \\ z \end{bmatrix} = \begin{bmatrix} c\theta_1\left[L_1+L_2\,c\left(\frac{\pi}{9}\right)+L_3c\left(\frac{\pi}{9}+\varphi\right)\right] \\ s\theta_1\left[L_1+L_2\,c\left(\frac{\pi}{9}\right)+L_3c\left(\frac{\pi}{9}+\varphi\right)\right] \\ -L_2s\left(\frac{\pi}{9}\right)-L_3s\left(\frac{\pi}{9}+\varphi\right) \end{bmatrix}
\tag{6}
$$

When $\Delta s \ge \Delta s1$:

$$
\begin{bmatrix} x \\ y \\ z \end{bmatrix} = \begin{bmatrix} c\theta_1\left[L_1+L_2\,c\left(\varphi-\frac{5\pi}{36}\right)+L_3c\left(\frac{\pi}{4}\right)\right] \\ s\theta_1\left[L_1+L_2\,c\left(\varphi-\frac{5\pi}{36}\right)+L_3c\left(\frac{\pi}{4}\right)\right] \\ -L_2s\left(\varphi-\frac{5\pi}{36}\right)-L_3s\left(\frac{\pi}{4}\right) \end{bmatrix}
\tag{7}
$$

ISSN: 2414-1895 DOI: 10.6919/ICJE.202605_12(5).0025

3.3 Inverse Kinematics Analysis of a Single Robot Leg

Inverse kinematics refers to the process of solving for the joint angles required to achieve a desired end-effector pose given the known pose coordinate system of the foot end. From Equations (6) and (7), it can be seen that θ_1 is only related to $x(\theta,\varphi)$and $y(\theta,\varphi)$, which can be simplified as:

$$\theta_1 = \arctan\frac{y(\theta,\varphi)}{x(\theta,\varphi)} \tag{8}$$

Substituting θ_2 and θ_3 into Equation (8), and then using the residual function along with the Jacobian matrix, the final inverse kinematics equations of the robot are obtained through Newton-Raphson iteration, as shown in Equations (9) and (10):

1) When the ankle joint has not reached the limit position:

$$\begin{cases} \theta_1 = \arctan\dfrac{y(\theta,\varphi)}{x(\theta,\varphi)} \\ \varphi = \arcsin\left(\dfrac{-z - L_2\sin 20^\circ}{L_3}\right) - \dfrac{2\pi}{9} \end{cases} \tag{9}$$

2) When the ankle joint has reached the limit position:

$$\begin{cases} \theta_1 = \arctan\dfrac{y(\theta,\varphi)}{x(\theta,\varphi)} \\ \varphi^* = \lim\limits_{k\to\infty}\left(\varphi_k + 0.6\dfrac{-f(\varphi_k)}{J(\varphi_k)}\right) \end{cases} \tag{10}$$

3.4 Foot-End Trajectory

The rationality of the foot-end trajectory determines the terrain adaptability, motion stability, and energy efficiency of the hexapod robot. Based on the previously established D-H kinematic model and the underactuated coupling relationship, a MATLAB simulation platform was used to carry out trajectory characteristic analysis of a single leg and cooperative motion range analysis of the hexapod.

From the trajectory simulation results (as shown in Fig. 4), it can be seen that the foot-end trajectory of the underactuated single leg exhibits a continuous, smooth, ellipse-like curve. The coverage in the X-Y plane matches the requirements of the body's lateral span and longitudinal step length, while the maximum travel in the Z-axis meets the typical obstacle-crossing requirement of 100 mm. The smoothness of the trajectory originates from the cable-driven torsion-spring coupling mechanism of the underactuated joints, which effectively avoids the abrupt trajectory changes caused by rigid transmission, providing a foundation for stable robot locomotion. Moreover, the trajectory shows a gentle arc characteristic during the stance phase, which reduces impact between the foot end and the ground and improves motion compliance.

The point cloud map (as shown in Fig. 5) visually presents the overall reachable workspace of the hexapod robot's foot ends. The coverage in the X-axis (forward-backward direction) satisfies the step length requirements for long-distance travel, the span in the Y-axis (lateral direction) ensures the body's lateral stability, and the vertical travel in the Z-axis adapts to changes in terrain height. From the point cloud distribution density, there is a reasonable overlapping area among the motion ranges of the six legs, providing redundancy for gait switching and terrain adaptability adjustments. The reachable regions of all foot ends do not exceed the body's structural constraints, and there is no risk of motion interference, verifying the rationality of the leg structure dimensions and layout design.

ISSN: 2414-1895 DOI: 10.6919/ICJE.202605_12(5).0025

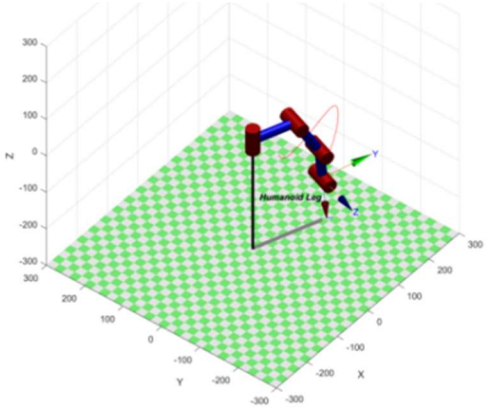

Fig. 4 Foot-end trajectory

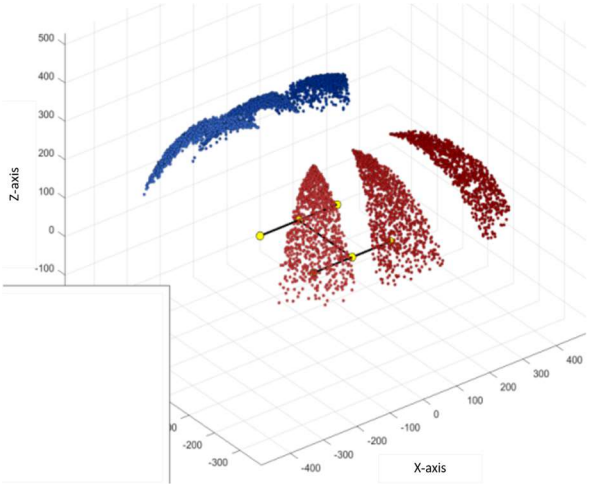

Fig. 5 Point cloud map of the motion range

4. Straight-Line Gait

Due to the special constraints imposed by the underactuated mechanism on the leg structure design, the robot must adopt a basic gait pattern to achieve stable motion. This robot uses the tripod gait as the basic gait strategy for straight-line locomotion. For ease of description, the six legs of the hexapod robot are denoted as L1, L2, L3, R1, R2, and R3, as shown in Fig. 6, which is a diagram of the leg grouping.

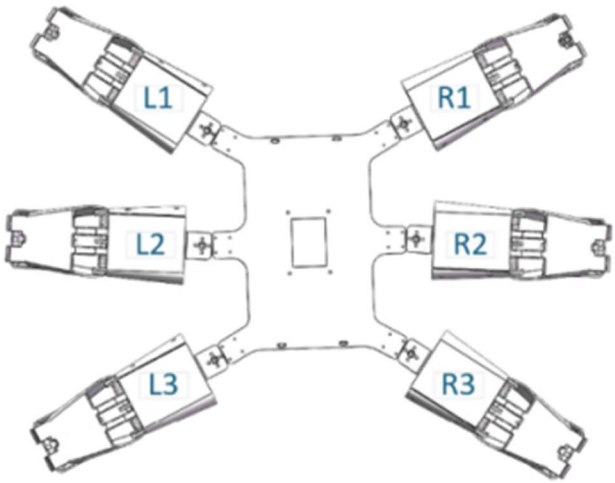

Fig. 6 Leg grouping diagram

ISSN: 2414-1895 DOI: 10.6919/ICJE.202605_12(5).0025

In the tripod gait, the hexapod robot is divided into two groups: L1, L3, and R2 form one group, while L2, R1, and R3 form the other group. The two groups of legs alternately act as the support phase and the swing phase. The swing phase duration is set to 1 second, and the support phase duration is set to 2 seconds to enhance body stability. Fig. 7 shows the gait phase diagram of the underactuated hexapod robot.

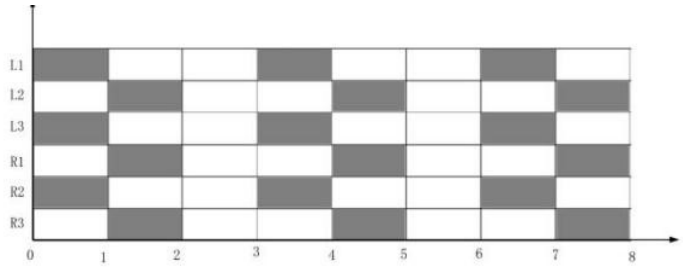

Fig. 7 Tripod gait phase diagram

5. ADAMS Dynamics Model Simulation

Using ADAMS software, a multi-body dynamics model of the underactuated hexapod robot was established, with the necessary constraints and drives added. Kinematic analysis of the relevant components was carried out to provide parameter references for the design and manufacturing of the physical prototype [13].

By analyzing the motion state of the center-of-mass (CoM) displacement of the underactuated hexapod robot during straight-line locomotion, the stability of the underactuated legged robot can be evaluated. Fig. 8 shows the CoM displacement curve of the underactuated hexapod robot. From the CoM displacement curve, it can be observed that the underactuated hexapod robot is relatively stable overall. The x-axis direction corresponds to the left-right direction of the robot, where the displacement curve shows small fluctuations. The y-axis direction is the vertical direction. When moving forward without obstacles, the robot exhibits no significant bouncing. The simulation results fully demonstrate that the bionic hexapod robot can move smoothly in the intended direction without oscillation or deviation.

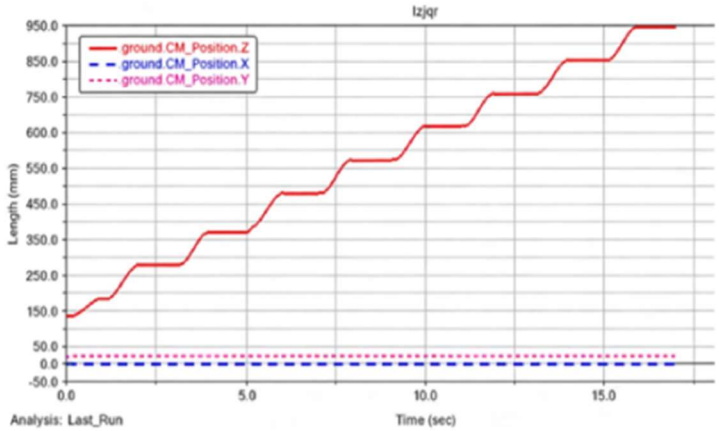

Fig. 8 Center-of-mass displacement curve of the underactuated hexapod robot

As shown in Figs 9 and 10, the angular velocity and angular acceleration of the three joints are presented respectively. The three curves in the data plots correspond to the angular velocity and angular acceleration of the ankle, knee, and hip joints. From the data plots, it can be seen that for the same joint in different leg groups, the velocity curves have the same magnitude, with their timing regularly staggered. The angular acceleration curves show that the angular acceleration of each joint

ISSN: 2414-1895 DOI: 10.6919/ICJE.202605_12(5).0025

changes smoothly and continuously throughout the entire gait cycle, with no abrupt changes or high-frequency oscillations. Only small, controllable peaks appear during the cable-driven switching phases. The simulation results indicate that there is no significant impact in joint motion, verifying the compatibility and motion stability of the designed underactuated mechanism with the tripod gait.

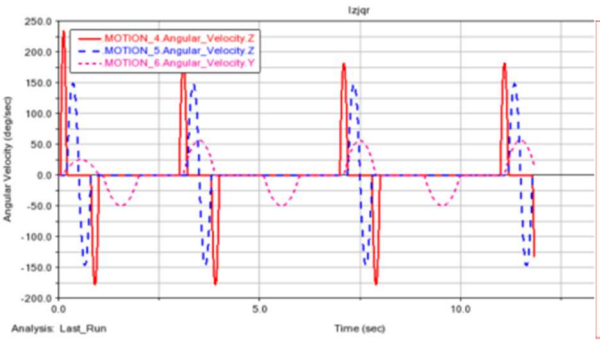

Fig. 9 Angular velocity of the three joints

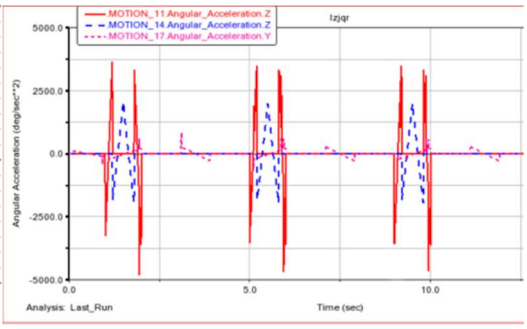

Fig. 10 Angular acceleration of the three joints

Fig 11 shows the torque curves of servo A at the hip joint of the mechanical leg and servo B inside the thigh. The simulation results indicate that both torques remain within the rated torque range of the servos. Fig. 12 shows the torque of the torsion springs: the solid line represents the torque of the torsion spring at the knee joint, and the dashed line represents the torque of the torsion spring at the ankle joint. From the simulated torsion spring torque curves of the knee and ankle joints, it can be seen that the torsion springs rapidly generate a reverse restoring torque during the leg-lowering ground-contact phase, reaching a peak at the moment of foot-ground impact, effectively absorbing and buffering the collision energy. During the leg-lifting phase, the torque increases approximately linearly with the joint angle.

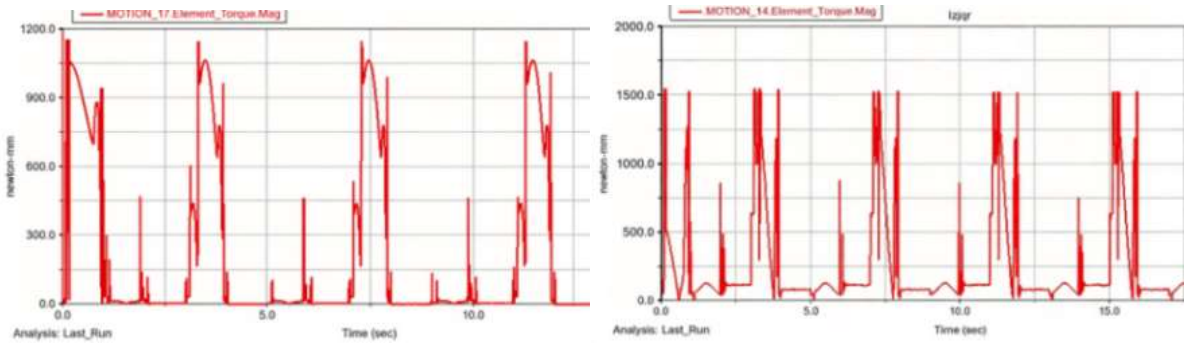

Fig. 11 Servo torque curves

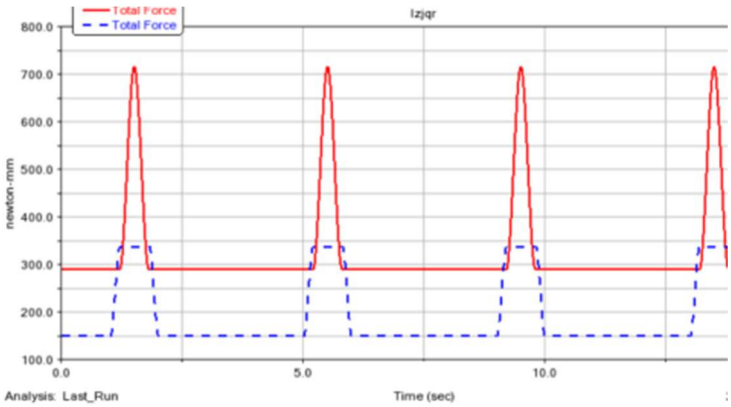

Fig. 12 Torsion spring torque curves

ISSN: 2414-1895 DOI: 10.6919/ICJE.202605_12(5).0025

6. Prototype Walking Experiment

A three-dimensional model of the underactuated hexapod robot was established using SolidWorks, and a physical prototype of the underactuated hexapod robot was manufactured and assembled (as shown in Fig. 13). The prototype was mainly fabricated via 3D printing using ABS material, ensuring light weight and structural strength. The drive system consists of 12 digital servos, and the ankle joint limit mechanism as well as the torsion springs were installed according to the design parameters. The cable-driven transmission system uses high-strength polyethylene fiber rope to ensure reliable power transmission.

Fig. 13 Underactuated hexapod robot prototype

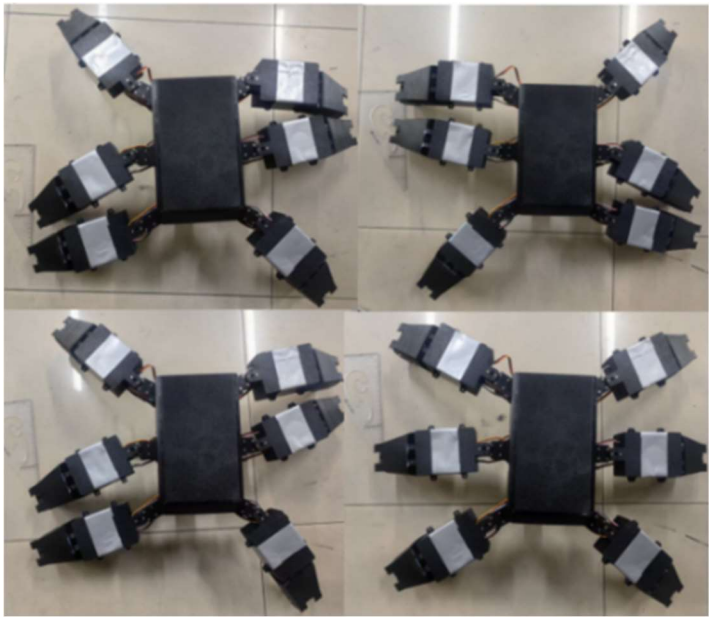

Fig. 14 Straight-line gait experiment

A straight-line motion test was carried out on flat ground with the prototype. A pre-planned tripod gait program was embedded in the control system to drive the two leg groups to swing and support alternately. Experiments show that the developed underactuated hexapod robot prototype is capable of stable straight-line walking. As shown in Fig. 14, during a complete gait cycle, the legs in the swing phase (e.g., the right front, left middle, and right rear legs in the figure) can successfully

ISSN: 2414-1895 DOI: 10.6919/ICJE.202605_12(5).0025

complete the “lift-forward-place” motion sequence under the action of the cable-driven torsion-spring coupling mechanism. Meanwhile, the other three legs in the support phase stably support the body to move forward. The entire motion process is coherent, with no obvious body overturning or violent shaking, demonstrating the feasibility of the underactuated leg mechanism design in physical implementation and its compatibility with the tripod gait.

7. Conclusion

To address the issues of complex actuation and high power consumption in conventional hexapod robots, an underactuated leg mechanism based on cable-driven torsion-spring coupling is designed. In this design, a single servo drives both the knee and ankle joints in a coupled manner, reducing the number of actuators per leg to two, thereby achieving lightweight structure and simplified control.

A kinematic model is established using the D-H parameter method. Smooth foot-end trajectories are obtained through MATLAB simulation, and dynamic verification is carried out using ADAMS. Simulation results show that the mechanism exhibits stable motion under the tripod gait, continuous joint motion, effective impact buffering by the torsion springs, and servo torques that meet expectations. This study provides a novel underactuated mechanism design for low-cost, highly adaptable hexapod robots, which has good application prospects in unstructured environments.

Acknowledgments

This work was supported by Tianjin Key R&D Program - Institute-City Cooperation Project (24YFYSHZ00090), Key Project of Natural Science under the Scientific Research Program of Tianjin Municipal Education Commission (2022ZD032).

References

[1] Robots Deployed in Search Operation Following Deadly Russian Coal Mine Explosion(VIDEO)[EB/OL].[2024-11-02].

[2] Choi B, Lee W, et al. Development and Control of a Military Rescue Robot for Casualty Extraction Task[J]. Journal of Field Robotics, 2019, 36(4): 656-676.

[3] Z. Li, S.Y. Wu, et al. Research and Design of a Bionic Spider Robot for Railway Geological Detection[J]. Mechanical Engineer, 2024(08): 120-122+126.

[4] Liu Y, Ben-Tzvi P, et al. Systematic development of a novel, dynamic, reduced complexity quadruped robot platform for robotic tail research[C]//2022 International Conference on Robotics and Automation (ICRA). IEEE, 2022: 4664-4670.

[5] ZHAO J, GAO J, et al. A Search-and-Rescue Robot System for Remotely Sensing the Underground Coal Mine Environment[J]. Sensors, 2017, 17(10): No. 24-26.

[6] Q.G. Zhu. "Jueying" Robot Assists Smart Security[J]. China Surveying and Mapping, 2019: 31-33.

[7] SATO Y, KAKUTO T, TANAKA T, et al. Development of a radioactive substance detection system integrating a Compton camera and a LiDAR camera with a hexapod robot[J]. Nuclear Instruments and Methods in Physics Research Section A: Accelerators, Spectrometers, Detectors and Associated Equipment, 2024: 169-300.

[8] Davliakos I, Roditis I L, Lika K, et al. Design, development, and control of a tough electrohydraulic hexapod robot for subsea operations[J]. International Journal of the Robotics Society of Japan, 2018, 32(9al0): 234-256.

[9] Buchanan R, Wellhausen L, Bjelonic M, et al. Perceptive whole body planning for multilegged robots in confined spaces[J]. Journal of Field Robotics, 2021, 38(1): 68-84.

[10] Y.H. Zhang, Y.W. Qian, H. Lu. Structural Design of a Hexapod All-terrain Robot[J]. Modern Machinery, 2021(05): 8-11.

[11] H.Y. Ren, Q.M. Li, J.X. Jiang. Design and Analysis of a Novel Elastic Leg Structure for Legged Robots[J]. Mechanical Science and Technology, 2018, 37(03): 372-379.

ISSN: 2414-1895 DOI: 10.6919/ICJE.202605_12(5).0025

[12] B. Pan, B.W. Chen. Research on Project-driven Robotics Course Teaching[J]. Modern Manufacturing Technology and Equipment, 2023, 59(2): 213-215.

[13] Y.J. Zhang, Y.K. Yang, Z.X. Xiao, et al. Dynamic Simulation Analysis of a Hexapod Ant-inspired Bionic Robot[J]. Machinery Design & Manufacture, 2024(11): 83-87+92.